Unreliability Tracing of Power Systems for Identifying the Most Critical Risk Factors Considering Mixed Uncertainties in Wind Power Output

Siying Zhao, Changzheng Shao, *Member*, *IEEE*, Jinfeng Ding, Bo Hu, *Senior Member*, *IEEE*, Kaigui Xie, *Senior Member*, *IEEE*, Xueying Yu, and Zihan Zhu

***Abstract*—For conventional power systems, the forced outage of components is the major cause of load shedding. Unreliability tracing is utilized to allocate the total system load-shedding risk among individual components in accordance with their different contributions. Therefore, critical components are identified and pertinent measures can be taken to improve system reliability. The integration of wind power introduces additional risk factors into power systems, causing previous unreliability tracing methods to become inapplicable. In this paper, a novel unreliability tracing method is proposed that considers both aleatory and epistemic uncertainties in wind power output and their impacts on power system load-shedding risk. First, modelling methods for wind power output considering aleatory and epistemic uncertainties and component outages are proposed. Then, a variance-based index is proposed to measure the contributions of individual risk factors to the system load-shedding risk. Finally, a novel unreliability tracing framework is developed to identify the critical factors that affect power system reliability. Case studies verify the ability of the proposed method to accurately allocate load-shedding risk to individual risk factors, thus providing decision support for reliability enhancement.**

***Index Terms*—Unreliability tracing, epistemic uncertainty, wind power, multisource heterogeneous risk factors.**

NOMENCLATURE

A. Abbreviations

ANOVA	analysis of variance
FOD	frame of discernment
BPA	basic probability assignment
EFE	extended focal element
CDF	cumulative distribution function
EENS	expected energy not supplied
MCS	Monte Carlo simulation
FOR	forced outage rate
MTTF	mean time to failure
MTTR	mean time to repair

B. Variables

k, k'	indices of two different intervals for wind power forecast error
t, v, k_{sam}, o	indices of time, risk factors, samples, sample set columns
i, i'	indices of two different buses
k_{age}, k_{com}, j	indices of ageing failure rates, state segments, components
g, w	indices of thermal, wind power units
$\boldsymbol{\Theta}$, $\boldsymbol{A}$	set, subset of intervals for wind power forecast error
$\boldsymbol{\Theta}_{\text{ex}}$	set of extended focal elements
$\boldsymbol{x}$, $\boldsymbol{y}$, $\boldsymbol{x}'$, $\boldsymbol{y}'$	sets, complementary sets of two different risk factor samples
$\boldsymbol{u}_1$, $\boldsymbol{u}_2$, $\boldsymbol{u}_3$	sets of random variables representing aleatory uncertainty, epistemic uncertainty, component outage
$\boldsymbol{\zeta}^1$, $\boldsymbol{\zeta}^2$, $\boldsymbol{\zeta}^3$	two different sample sets and the combined sample set of them
$\boldsymbol{\eta}^{(v)}$	sample set constructed for risk factor x_v
$\boldsymbol{h}_{\text{ieq}}$, $\boldsymbol{h}_{\text{eq}}$	sets of inequality, equality constraints
$\boldsymbol{\theta}$, $\boldsymbol{B}$, $\boldsymbol{T}$	sets of bus phase angles, buses, time intervals

Received: October 3, 2023
Accepted: May 11, 2024
Published Online: September 1, 2024

Siying Zhao is with the Hubei Electric Power Planning, Design and Research Institute Co., Ltd., Wuhan 430040, China (e-mail: cquzhaosiying@foxmail.com).

Changzheng Shao (corresponding author), Bo Hu, Kaigui Xie, Zihan Zhu are with the State Key Laboratory of Power Transmission Equipment Technology, School of Electrical Engineering, Chongqing University, Chongqing 400044, China (e-mail: cshao@cqu.edu.cn; hboy8361@163.com; kaiguixie@vip.163.com; hanzizhu2008@126.com).

Jinfeng Ding is with the State Grid Chengdu Electric Power Supply Company, Chengdu 610000, China (e-mail: dingjf7@foxmail.com).

Xueying Yu is with the School of Electrical Engineering, Sichuan University, Chengdu 610065, China (e-mail: scuyuxueying@foxmail.com).

DOI: 10.23919/PCMP.2023.000022

$\boldsymbol{P}^{\mathrm{tu}}$, $\boldsymbol{P}^{\mathrm{wind}}$ sets of thermal, wind power unit outputs

$\boldsymbol{P}^{\mathrm{cur}}$ set of electric load shedding

$\boldsymbol{G}$, $\boldsymbol{W}$ sets of thermal, wind power units

$P_1^{\mathrm{wind}}, F^{\mathrm{wind}}, e^{\mathrm{wind}}$ real value, forecast value, forecast error of wind power output

$e_k^{\mathrm{wind}}, e_{k+1}^{\mathrm{wind}}$ minimum, maximum values in interval k of wind power forecast error

$e_1^{\mathrm{wind}}, e_{N+1}^{\mathrm{wind}}$ lower, upper boundaries of wind power forecast error

d, E_k, H interval width, interval k, extended focal element of wind power forecast error

$N, N_\lambda, N_{\mathrm{age}}, N_{\mathrm{obj}}, N_{\mathrm{sam}}, N_{\mathrm{com}}, N_{\mathrm{bus}}$ numbers of intervals of wind power forecast error, wind conditions, ageing failure rates, risk factors, samples, component state segments, buses

m, m_1, m_2 basic probability assignments for wind power forecast error, offset of failure rate, ageing failure rate

P, Bel, Pl cumulative distribution, belief, plausibility functions of wind power forecast error

$\lambda_{\text{wind-ep}}, \lambda_{\mathrm{wind}}, \lambda_{\mathrm{ep}}$ real value, constant value, offset of wind power unit failure rates

$\lambda_{\text{com-age}}, \lambda_{\mathrm{com}}, \lambda_{\mathrm{age}}$ real, constant, ageing failure rates of components

$V_w, P_{\mathrm{mean},w}^{\mathrm{wind}}$ wind variability index, average output of wind power unit w

κ_1, κ_2 shape, scale parameters of Weibull distribution

Y, $g(\boldsymbol{x})$ unreliability index, unreliability index function of sample x

x_v, S_v, D_v vth risk factor, unreliability tracing index of risk factor x_v, variance of risk factor x_v

g_0, D expectation, variance of unreliability index function $g(x)$

u_1^w, u_2^w, u_3^j random variables representing aleatory uncertainty of wind power unit w, epistemic uncertainty of wind power unit w, outage of component j

T, T_{com} sample period, length of component state sequence

$\gamma_j, \xi_j, \lambda_j, \partial_{j,k_{\mathrm{com}}}, s_j$ random number to simulate state duration, state duration, state transition rate, state segment k_{com}, state of component j

$\theta_{i,t}, \theta_{i',t}$ phase angles of buses i, i' at time t

$X_{i,i'}, F_{i,i'}^{\max}$ reactance, maximum capacity of transmission line connecting buses i and i'

$s_{ii',t}, s_{g,t}, s_{w,t}$ states of the transmission line connecting buses i and i', thermal unit g, wind power unit w at time t

$P_g^{\mathrm{tu,min}}, P_g^{\mathrm{tu,max}}, P_{w,t}^{\mathrm{wind,min}}, P_{w,t}^{\mathrm{wind,max}}$ minimum, maximum outputs of thermal unit g, wind power unit w at time t

U_g, R_g upwards, downwards ramping capabilities of thermal unit g

$\theta_i^{\max}$ maximum phase angle of bus i

$P_{g,t}^{\mathrm{tu}}, P_{g,t-\Delta t}^{\mathrm{tu}}$ outputs of thermal unit g at time t, $t-\Delta t$

$P_{w,t}^{\mathrm{wind}}, P_{i,t}^{\mathrm{load}}$ outputs of wind power unit w, power load of bus i at time t

$\sigma(S_v), \overline{S}_v$ standard deviation, mean of S_v

$\varepsilon, \varepsilon_{\mathrm{set}}$ maximum, convergence variability coefficients of S_v

I. Introduction

Several major blackouts have occurred in recent years, such as the power outage in Texas in February 2021 caused by the forced outage of generators due to extreme cold weather [1] and another instance in California in August 2020 that resulted from a tripped gas-fired unit [2]. Such incidents illustrate that the forced outage of devices may have serious consequences for power systems, including widespread emergency load shedding [3]–[5].

A modern power system consists of a vast number of electrical devices responsible for electricity generation, transmission, distribution, and so on. Each device can be regarded as a component for power system unreliability evaluation and tracing. Identification of the critical components that contribute most of the system load-shedding risk is highly valuable. The results of such analysis can be used in the allocation of maintenance resources, equipment selection, and reinforcement planning to improve system reliability under a limited budget [6].

Considering the potentially significant role that critical component identification can play, several pioneering studies have been conducted on this topic, which can be divided into three categories: sensitivity analysis methods, electric-betweenness-based methods, and unreliability tracing methods.

Sensitivity analysis methods focus on determining the importance of components by calculating the change rate of the system unreliability index relative to component reliability parameters [7]–[9]. The electric-betweenness-based methods use complex network theory to determine the critical components of the system [10]–[12]. However, sensitivity analysis methods have difficulty analysing the influence of different components in large-scale systems and high contingency-level outage events, while electric-betweenness-based methods significantly simplify the operation state and electrical characteristics of power systems and require reanalysis of

the network topology when it changes. In addition, the above two types of methods have difficulty quantifying the contributions of different components to the system unreliability index and judging the primary and secondary contributions of components to system risk.

Unreliability tracing methods, inspired by the similar idea of power flow tracing for transmission loss allocation problems, make it possible to attribute system load-shedding risk to specific components [13], [14]. In this way, the identification of critical components can be realized efficiently and comprehensively. In [13], the proportional allocation principle was first proposed for unreliability tracing. A relatively high unreliability tracing index for a component indicates a significant impact on the system load-shedding risk. In [14], the system load-shedding risk is allocated to each component based on the improved Shapley value.

Recently, wind power has developed rapidly to achieve clean, efficient, and sustainable energy system development and dual-carbon goals [15], [16]. The large-scale integration of wind power has led to enormous changes in the unreliability analysis of power systems, as wind power output uncertainty has become another major cause of system load-shedding risk [17], [18]. There are two types of uncertainties related to wind power output [19], [20]. Aleatory uncertainty is due to the inherent volatility of wind speed and wind power, whereas epistemic uncertainty results from modelling error caused by a lack of data/knowledge [21]–[23]. Wind power output uncertainties are completely different from component outages in terms of modelling and analysis. Hence, traditional unreliability tracing methods are difficult to apply to power systems with a high level of wind power penetration [24], [25].

The relationship between system load-shedding risk and multisource heterogeneous risk factors, including wind power output uncertainty and component outage, is shown in Fig. 1. In power systems integrated with wind power, multisource heterogeneous risk factors are the major causes of system load shedding, and unreliability tracing can be utilized to allocate the system load-shedding risk to individual risk factors for each component.

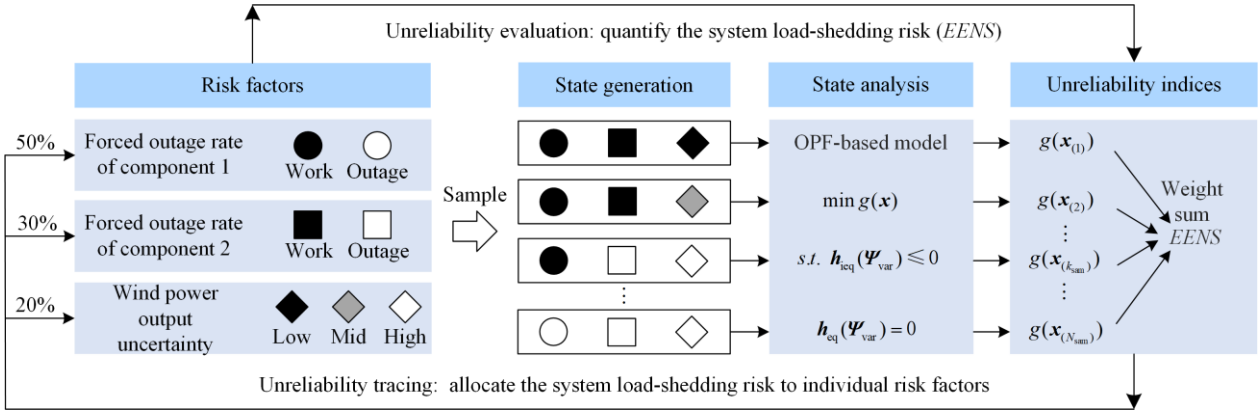

Fig. 1. The relationship between unreliability evaluation and tracing of power systems.

To address the current research gap, a novel unreliability tracing method is proposed in this paper to allocate system load-shedding risk to not only component outages but also the aleatory and epistemic uncertainties of wind power output, which cannot be allocated via traditional unreliability tracing methods. First, the multisource heterogeneous risk factors are modelled for system unreliability allocation. Second, an unreliability tracing index based on analysis of variance (ANOVA) is first proposed to measure the contributions of individual risk factors to the system load-shedding risk. Finally, an unreliability tracing framework is developed to identify the critical factors of the power system and provide theoretical bases and suggestions for system reliability enhancement.

If the aleatory uncertainty of wind power output has a great impact on system load-shedding risk, it can be reduced by employing additional electricity reserves, participating in the auxiliary market, installing energy storage equipment, and other means. If the epistemic uncertainty of wind power output has a more significant impact on system load-shedding risk, system operators can be encouraged to work on developing more accurate wind power forecast methods.

The rest of the paper is presented as follows. Section II delineates the models for multisource heterogeneous risk factors. Section III introduces the ANOVA-based unreliability tracing method, and section IV describes the unreliability tracing framework for power systems integrated with wind power. Section V presents case studies and conclusions are given in section VI.

II. Modelling of Wind Power Output and Component Reliability

The analysis and modelling of risk factors that contribute to the system load-shedding risk are the basis of unreliability tracing. In this section, wind power output is first modelled considering both aleatory and epistemic uncertainties. Then, reliability models of different types of components are developed.

A. Wind Power Output Model Considering Aleatory and Epistemic Uncertainties

Wind power is significantly affected by meteorological conditions. Therefore, it is virtually impossible to achieve a perfect forecast of wind power output without any error. The wind power forecast error represents the characteristic uncertainty between the forecast value and the real value. The relationships between the real value P_1^{wind}, the forecast value F^{wind}, and the forecast error e^{wind} of the wind power output are as follows:

$$P_1^{\text{wind}} = F^{\text{wind}} + e^{\text{wind}} \tag{1}$$

Probability distribution fitting is a common method of describing the aleatory uncertainty related to the forecast error. The wind power forecast error has commonly been assumed to be a nearly Gaussian distribution [26]. Through statistical analysis, the parameters of the Gaussian distribution that describe the wind power forecast error can be calculated [27].

However, the Gaussian distribution established in this way could be significantly different from the real distribution of the wind power forecast error. The reasons are twofold. First, the wind power forecast error may not follow any particular distribution in reality [28], [29]. Hence, modelling the forecast error as a Gaussian distribution or any other standard distribution will result in errors. Second, there may not be sufficient data to accurately estimate the parameters of the distribution model even if the forecast error follows a standard distribution [30]. These two reasons explain the existence of epistemic uncertainty related to wind power forecast.

Accordingly, the wind power forecast error model considering both aleatory and epistemic uncertainties [30] is introduced in this section. First, the range of the wind power forecast error is divided into N intervals as follows:

$$e_k^{\text{wind}} = e_1^{\text{wind}} + (k-1)d,\ k \in \{1,2,\cdots,N\} \tag{2}$$

$$d = (e_{N+1}^{\text{wind}} - e_1^{\text{wind}})/N \tag{3}$$

where k and d denote the indices of different intervals and the width of each interval, respectively; e_k^{wind} represents the minimum value in the interval k of the wind power forecast error; and e_1^{wind} and e_{N+1}^{wind} represent the lower and upper boundaries of the forecast error, respectively.

1) Frame of Discernment

Each interval $\left[e_k^{\text{wind}}, e_{k+1}^{\text{wind}}\right]$ is referred to as a basic element represented by E_k. The frame of discernment (FOD) $\boldsymbol{\Theta}$ is the set of all E_k:

$$\boldsymbol{\Theta} = \{E_1, E_2, \cdots, E_N\} \tag{4}$$

The power set of $\boldsymbol{\Theta}$ is $2^{\boldsymbol{\Theta}}$, and any subset $\boldsymbol{A}$ of $\boldsymbol{\Theta}$ can be represented as an event containing possible wind power forecast errors belonging to $2^{\boldsymbol{\Theta}}$:

$$\boldsymbol{A} \in 2^{\boldsymbol{\Theta}} = \left\{ \begin{matrix} \{\varnothing\}, \{E_1\}, \{E_2\}, \cdots, \\ \{E_1, E_2, \cdots, E_k\}, \{E_1, E_3, \cdots, E_{k+1}\}, \cdots, \boldsymbol{\Theta} \end{matrix} \right\} \tag{5}$$

2) Basic Probability Assignment

A basic probability assignment (BPA), which is also known as a mass function m, is introduced to assign the probability to each subset $\boldsymbol{A}$:

$$\sum_{\boldsymbol{A} \in 2^{\boldsymbol{\Theta}}} m(\boldsymbol{A}) = 1 \tag{6}$$

$$m(\boldsymbol{A}) \geqslant 0 \tag{7}$$

$$m(\varnothing) = 0 \tag{8}$$

Equation (6) indicates that the cumulative probability sum of all subsets equals 1. Equation (7) indicates that the probability of any subset $\boldsymbol{A}$ cannot be negative. Equation (8) indicates that an empty set is meaningless; thus, the BPA of $\varnothing$ is zero. Any subset $\boldsymbol{A}$ satisfying $m(\boldsymbol{A}) > 0$ is referred to as a focal element. Considering the characteristics of the wind power forecast error and the lack of historical data, some subsets satisfying $m(\boldsymbol{A}) = 0$ must be considered to ensure the accuracy of the wind power forecast error model. Therefore, the set of extended focal elements (EFEs) $\boldsymbol{\Theta}_{\text{ex}}$ is proposed to represent the union of focal elements and basic elements.

3) Belief Function and Plausibility Function

To describe epistemic uncertainty, it is reasonable to extend the probability distribution of the wind power forecast error to a banded probability interval. The belief function *Bel* is defined as the lower probability boundary, whereas the plausibility function *Pl* is defined as the upper probability boundary. Based on the BPA m in FOD $\boldsymbol{\Theta}$, *Bel* and *Pl* can be calculated as follows:

$$Bel(H_1) = \sum_{H_2 \subseteq H_1} m(H_2), \forall H_1, H_2 \in \boldsymbol{\Theta}_{\text{ex}} \tag{9}$$

$$Pl(H_1) = \sum_{H_2 \cap H_1 \neq \varnothing} m(H_2), \forall H_1, H_2 \in \boldsymbol{\Theta}_{\text{ex}} \tag{10}$$

where H_1 and H_2 represent two different EFEs.

As shown in Fig. 2, the aleatory uncertainty indicates that the wind power forecast error may belong to any EFE. The epistemic uncertainty of any EFE $H_k (H_k \in \boldsymbol{\Theta}_{\text{ex}})$ can be expressed by the belief interval $\left[Bel(H_k), Pl(H_k)\right]$, where the bandwidth depends on the known information.

Based on the cumulative distribution function (CDF), the uncertainty model of wind power forecast error can be established as follows:

$$0 \leqslant Bel\left(\{E_1, \cdots, E_k\}\right) \leqslant P\left(E_k\right) \leqslant Pl\left(\{E_1, \cdots, E_k\}\right) \leqslant 1 \tag{11}$$

where $P(E_k)$ represents the CDF of E_k.

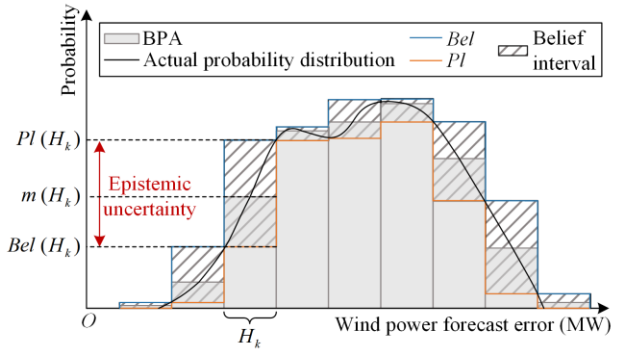

Fig. 2. Schematic diagram of *Bel* and *Pl*.

After the construction and fusion of multisource information [30], a precise BPA can be obtained through the fusion of historical data and expert information. Then, the improved BPA can be used for the calculation of *Bel* and *Pl* in (11), and a modified wind power forecast model considering multisource information can be further obtained. Finally, in combination with (1), the wind power output model considering both aleatory and epistemic uncertainties is formulated.

B. Reliability Model of Wind Power Units

Due to intermittent and fluctuations in wind speed, the degree and frequency of the load ratio variability of wind power units are much greater than those of conventional components, and the forced outages of electronic components inside wind power units is very sensitive to frequent fluctuations.

With the rapid development of wind power in recent years, the number and capacity of wind farms have been increasing rapidly, and their operation situation is changing rapidly. As a result, the available statistical samples for the unreliability evaluation of wind farms are limited. At present, the commonly used reliability parameters for wind farms are estimated based on military manuals [31]. However, the reliability differs between different regions and different types of wind farms; thus, the reliability level is difficult to estimate accurately and effectively via the military-manual-based method. The application of general estimation formulas will lead to great epistemic uncertainty.

Therefore, it is necessary to model the failure rate $\lambda_{\text{wind-ep}}(t)$ of wind power units varying with time t considering wind scenarios:

$$\lambda_{\text{wind-ep}}(t)=\lambda_{\text{wind}}+\lambda_{\text{ep}}(t) \tag{12}$$

where λ_{wind} and $\lambda_{\text{ep}}(t)$ represent the constant value and offset of the wind power unit failure rate, respectively.

The typical wind variability index V_w and the average output $P_{\text{mean},w}^{\text{wind}}$ of wind power unit w are selected to form N_λ typical pairwise operating conditions [32]. The offset boundary of the wind power unit failure rate is obtained based on all typical V_w and $P_{\text{mean},w}^{\text{wind}}$ pairs. Based on the uncertainty model in section II.A, the BPA m_1 with N_λ EFEs can be established as follows:

$$m_1(H)=\frac{1}{N_\lambda} \tag{13}$$

Based on the methods of expert information construction and multisource information fusion in section II.A, the fused BPA for the offset of the wind power unit failure rate can be obtained.

C. Reliability Model of the Ageing Components

The reliability of components is affected by various external and internal factors, such as meteorological factors, load rate, and health status. Thus, the components' reliability parameters change dynamically. For ageing components such as transmission lines, the failure rate of ageing components $\lambda_{\text{com-age}}(t)$ can be divided into a constant failure rate λ_{com} and an ageing failure rate $\lambda_{\text{age}}(t)$ [33]:

$$\lambda_{\text{com-age}}(t)=\lambda_{\text{com}}+\lambda_{\text{age}}(t) \tag{14}$$

It is generally believed that the Weibull distribution can perfectly describe the change in the ageing failure rate of a component throughout its whole life cycle [34]. Based on the Weibull distribution, the ageing failure rate can be expressed as follows:

$$\lambda_{\text{age}}(t,\kappa_1,\kappa_2)=(\kappa_1/\kappa_2)(t/\kappa_2)^{\kappa_1-1} \tag{15}$$

where κ_1 and κ_2 represent the shape and scale parameters of the Weibull distribution, respectively.

However, the ageing outage mechanism of components is extremely complex and has numerous influencing factors. Although the Weibull distribution is applicable from a statistical perspective, the epistemic uncertainty of parameters cannot be avoided [35].

The probability box model combining the probability model and the interval model is utilized to represent this epistemic uncertainty by defining the upper and lower boundaries of variables in the form of CDFs [36].

This approach is suitable for variables with known boundary distribution functions such as the ageing failure rate of components.

Let the intervals of the shape parameter and scale parameter be $\kappa_1\in\left[\underline{\kappa}_1,\overline{\kappa}_1\right]$ and $\kappa_2\in\left[\underline{\kappa}_2,\overline{\kappa}_2\right]$, where $\underline{\kappa}_1$, $\overline{\kappa}_1$ and $\underline{\kappa}_2$, $\overline{\kappa}_2$ represent the lower and upper boundaries of κ_1 and κ_2, respectively. Then, the epistemic uncertainty of the component ageing failure rate can be modelled as follows:

$$\underline{\lambda}_{\text{age}}(t)=\min\lambda_{\text{age}}(\kappa_1,\kappa_2) \tag{16}$$

$$\overline{\lambda}_{\text{age}}(t)=\max\lambda_{\text{age}}(\kappa_1,\kappa_2) \tag{17}$$

Therefore, the ageing failure rate of components can be characterized by the interval $\lambda_{\text{age}}\in\left[\underline{\lambda}_{\text{age}},\overline{\lambda}_{\text{age}}\right]$, where $\underline{\lambda}_{\text{age}}$ and $\overline{\lambda}_{\text{age}}$ represent the lower and upper boundary functions of λ_{age}, respectively.

The relationship between the probability box and the epistemic uncertainty is shown in Fig. 3. Figure 3 shows that the greater the difference between the upper and lower boundary functions is, the greater the epistemic uncertainty of the ageing failure rate of the components.

Similar to the wind power forecast error, the accuracy of the failure rate model of the ageing components can also be optimized based on multisource information. The probability box model of the ageing failure rate of components is discretized into finite pairs $(\lambda_{\text{age},1}, m_2(\lambda_{\text{age},1})),\cdots,(\lambda_{\text{age},N_{\text{age}}}, m_2(\lambda_{\text{age},N_{\text{age}}}))$. Here, any $\lambda_{\text{age},k_{\text{age}}}(1 \leqslant k_{\text{age}} \leqslant N_{\text{age}})$ denotes an interval and $m_2(\lambda_{\text{age},k_{\text{age}}})$ denotes the corresponding BPA of $\lambda_{\text{age},k_{\text{age}}}$. The probability box and the discretization process of the component ageing failure rate are shown in Fig. 3.

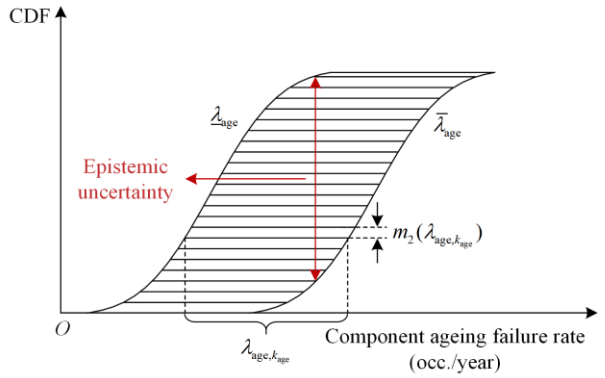

Fig. 3. The probability box and discretization process of the component ageing failure rate.

After the discretization process, the multisource information fusion method in section II.A can be utilized to correct the component ageing failure rate and calculate the corrected BPA.

III. Unreliability Tracing Idea Based on ANOVA

A. Decomposition of the Unreliability Index Function Based on ANOVA

Considering the mixed aleatory and epistemic uncertainties of wind power output and component outage, the unreliability index Y (such as the expected energy not supplied (EENS)) can be expressed as a function of the associated risk factors $x_1, x_2, \cdots, x_{N_{\text{obj}}}$:

$$Y = g(\boldsymbol{x}), \boldsymbol{x} = \left\{x_1, x_2, \cdots, x_{N_{\text{obj}}}\right\} \tag{18}$$

where $\boldsymbol{x}$ and N_{obj} are the set and number of risk factors, respectively.

Based on ANOVA theory [37], [38], the unreliability index function $g(\boldsymbol{x})$ can be decomposed into a sum of $2^{N_{\text{obj}}}$ subfunctions:

$$g(\boldsymbol{x}) = g_0 + \sum_{v=1}^{N_{\text{obj}}} g_v(x_v) + \sum_{1 \leqslant v < v' \leqslant N_{\text{obj}}} g_{w'}(x_v, x_{v'}) + \cdots + g_{1,2,\cdots,N_{\text{obj}}}(x_1, x_2, \cdots, x_{N_{\text{obj}}}) \tag{19}$$

where $v \in \left\{1, 2, \cdots, N_{\text{obj}}\right\}$ represents the index of different risk factors, constant g_0 represents the expectation value of the unreliability index function $g(\boldsymbol{x})$. $g_v(x_v)$, $g_{w'}(x_v, x_{v'})$, and $g_{1,2,\cdots,N_{\text{obj}}}(x_1, x_2, \cdots, x_{N_{\text{obj}}})$ represent the first-order subfunction of risk factor x_v, the second-order subfunction of risk factors x_v and $x_{v'}$, and the N_{obj}-order subfunction of all risk factors, respectively.

Equation (19) is called the ANOVA representation of $g(\boldsymbol{x})$ if the members in (20) are orthogonal and integrable, and satisfy the following relationship [37]:

$$\int_0^1 g_{v,\cdots,v'}(x_v, \cdots, x_{v'}) \mathrm{d}x_{v''} = 0, v \leqslant v'' \leqslant v' \tag{20}$$

Thus,

$$\int g(\boldsymbol{x}) \mathrm{d}\boldsymbol{x} = g_0 \tag{21}$$

Suppose that $g(\boldsymbol{x})$ is square integrable, square and integrate both sides of (19):

$$\int g^2(\boldsymbol{x}) \mathrm{d}\boldsymbol{x} = {g_0}^2 + \sum_{v=1}^{N_{\text{obj}}} \int g_v^2(x_v) \mathrm{d}x_v + \sum_{1 \leqslant v < v' \leqslant N_{\text{obj}}} \int g_{vv'}^2(x_v, x_{v'}) \mathrm{d}x_v \mathrm{d}x_{v'} + \cdots + \int g_{1,2,\cdots,N_{\text{obj}}}^2(x_1, x_2, \cdots, x_{N_{\text{obj}}}) \mathrm{d}x_1 \cdots \mathrm{d}x_{N_{\text{obj}}} \tag{22}$$

Thus, the variance expression of $g(\boldsymbol{x})$ can be obtained:

$$D = \sum_{v=1}^{N_{\text{obj}}} D_v + \sum_{1 \leqslant v < v' \leqslant N_{\text{obj}}} D_{vv'} + \cdots + D_{1,2,\cdots,N_{\text{obj}}} = \int g^2(\boldsymbol{x}) \mathrm{d}\boldsymbol{x} - g_0^2 \tag{23}$$

where D_v, $D_{vv'}$, and $D_{1,2,\cdots,N_{\text{obj}}}$ represent the variances of the first-order subfunction $g(x_v)$, the second-order subfunction $g_{vv'}(x_v, x_{v'})$, and the N_{obj}-order subfunction $g_{1,2,\cdots,N_{\text{obj}}}(x_1, x_2, \cdots, x_{N_{\text{obj}}})$, respectively.

B. Variance-based Unreliability Tracing Index

As described in section III.A, the variance of the unreliability index function $g(\boldsymbol{x})$ is decomposed into a sum of the variance contributions of individual risk factors and the combined variance contribution of different risk factors. To recognize the critical factors of power systems, it is necessary to investigate the independent contributions of individual risk factors to system unreliability. Therefore, the ratio of the variance attributable to individual risk factors to the total system variance is proposed as the unreliability tracing index, which is calculated as follows:

$$S_v = \frac{D_v}{D} \tag{24}$$

where S_v represents the unreliability tracing index of risk factor x_v. D_v can be obtained as follows [39]:

$$D_v = \int g(\boldsymbol{x})\left[g(x_v, \boldsymbol{y}') - g(\boldsymbol{x}')\right]\mathrm{d}\boldsymbol{x}\mathrm{d}\boldsymbol{x}' \tag{25}$$

where $\boldsymbol{y}$ represents the complementary set of x_v; thus, $\boldsymbol{x} = \{x_v, \boldsymbol{y}\}$. Similarly, x'_v and $\boldsymbol{y}'$ represent another sample of risk factor x_v and its complementary set, respectively; thus, $\boldsymbol{x}' = \{x'_v, \boldsymbol{y}'\}$.

Based on Monte Carlo simulation (MCS), two independent random points $\boldsymbol{x}_{(k_{\text{sam}})}$ and $\boldsymbol{x}'_{(k_{\text{sam}})}$ are sampled. After N_{sam} trials, g_0, D and D_v can be calculated [39]:

$$g_0 \approx \frac{1}{2N_{\text{sam}}}\sum_{k_{\text{sam}}=1}^{N_{\text{sam}}}\left[g(\boldsymbol{x}_{(k_{\text{sam}})}) + g(\boldsymbol{x}'_{(k_{\text{sam}})})\right] \tag{26}$$

$$D \approx \frac{1}{2N_{\text{sam}}}\sum_{k_{\text{sam}}=1}^{N_{\text{sam}}}\left[g^2(\boldsymbol{x}_{(k_{\text{sam}})}) + g^2(\boldsymbol{x}'_{(k_{\text{sam}})})\right] - g_0^2 \tag{27}$$

$$D_v \approx \frac{1}{N_{\text{sam}}}\sum_{k_{\text{sam}}=1}^{N_{\text{sam}}} g(\boldsymbol{x}_{(k_{\text{sam}})})\left[g(x_{v(k_{\text{sam}})}, \boldsymbol{y}'_{(k_{\text{sam}})}) - g(\boldsymbol{x}'_{(k_{\text{sam}})})\right] \tag{28}$$

where $k_{\text{sam}} \in \{1, 2, \cdots, N_{\text{sam}}\}$ and N_{sam} represent the index and number of samples, respectively. $x_{v(k_{\text{sam}})}$ and $\boldsymbol{y}_{(k_{\text{sam}})}$ represent sample k_{sam} of risk factor x_v and its complementary set, respectively; thus, $\boldsymbol{x}_{(k_{\text{sam}})} = \{x_{v(k_{\text{sam}})}, \boldsymbol{y}_{(k_{\text{sam}})}\}$. Similarly, $x'_{v(k_{\text{sam}})}$ and $\boldsymbol{y}'_{(k_{\text{sam}})}$ represent another sample k_{sam} of risk factor x_v and its complementary set, respectively; thus, $\boldsymbol{x}'_{(k_{\text{sam}})} = \{x'_{v(k_{\text{sam}})}, \boldsymbol{y}'_{(k_{\text{sam}})}\}$.

IV. Unreliability Tracing Framework for Power Systems Integrated with Wind Power

A. Generation of the Wind Power Output

The wind power forecast error includes both aleatory and epistemic uncertainties; thus, the traditional simulation methods are difficult to apply to the model in section II.A. Therefore, a two-layer MCS method is utilized to generate the wind power output sequence considering aleatory and epistemic uncertainties [30] as follows:

Step 1: The outer MCS process is used to randomly select the EFE to which the wind power forecast error sample value belongs.

This first step addresses the aleatory uncertainty of the wind power forecast error. A random number u_1^w uniformly distributed in [0, 1] is sampled for wind power unit w. Once u_1^w is given, the corresponding EFE can be obtained as follows:

$$e^{\text{wind}}(u_1^w) = \begin{cases} \left[e_1^{\text{wind}}, e_2^{\text{wind}}\right], 0 \leqslant u_1^w \leqslant P(E_1) \\ \vdots \\ \left[e_k^{\text{wind}}, e_{k+1}^{\text{wind}}\right], P(E_{k-1}) \leqslant u_1^w \leqslant P(E_k) \\ \vdots \\ \left[e_{k'}^{\text{wind}}, e_{k'+1}^{\text{wind}}\right], P(E_{k'-1}) \leqslant u_1^w \leqslant P(E_{k'}) \\ \vdots \\ \left[e_N^{\text{wind}}, e_{N+1}^{\text{wind}}\right], P(E_{N-1}) \leqslant u_1^w \leqslant 1 \end{cases} \tag{29}$$

where $1 \leqslant k \leqslant k' \leqslant N$.

Due to the epistemic uncertainty of wind power forecast errors, several P values may overlap. Thus, u_1^w may correspond to multiple continuous EFEs. Therefore, the lower boundary of E_k and the upper boundary of $E_{k'}$ are selected to generate the sample interval $\left[e_k^{\text{wind}}, e_{k'+1}^{\text{wind}}\right]$ for the outer MCS, and the width of the sample interval depends on the degree of epistemic uncertainty.

Step 2: The inner MCS process is used to randomly select the sample value of the wind power forecast error.

The second step addresses the epistemic uncertainty of the wind power forecast error. A random number u_2^w is sampled to determine the sample value e^{wind} of the wind power forecast error from the range $\left[e_k^{\text{wind}}, e_{k'+1}^{\text{wind}}\right]$:

$$u_2^w \in [0,1] \rightarrow e^{\text{wind}} \in \left[e_k^{\text{wind}}, e_{k'+1}^{\text{wind}}\right] \tag{30}$$

A diagram of the two-layer MCS process is shown in Fig. 4. The sample value of the wind power output is calculated via (1). A wind power output sequence can be obtained by repeating the above steps throughout the sample period T.

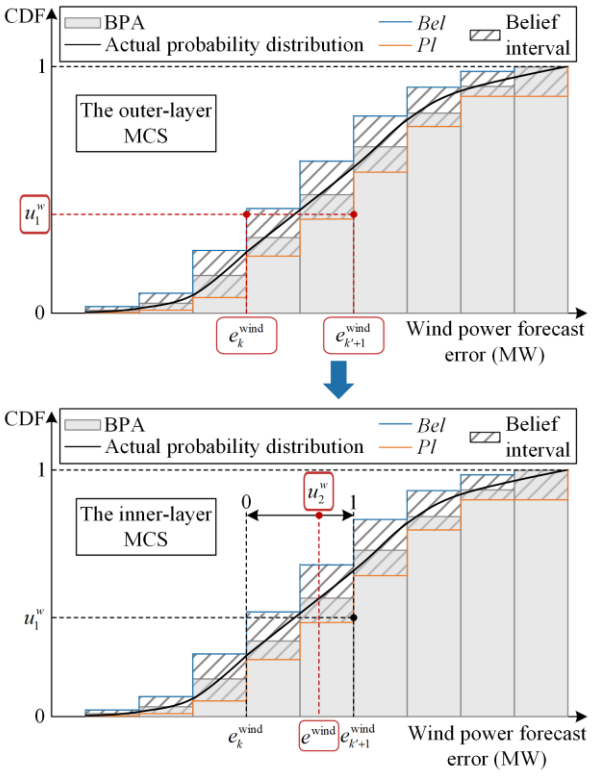

Fig. 4. Double-layer MCS in the generation of wind power output considering aleatory and epistemic uncertainties.

B. Generation of Component States (Outage or Work)

The sequential MCS method is utilized to simulate the component states to preserve the sequential characteristics of component outages.

It is assumed that each component has two possible states (outage or work), and all components are initially in the work state. A random number γ_j uniformly dis-

tributed in [0, 1] is used to simulate the state duration ξ_j of component j as follows:

$$\xi_j = -\frac{1}{\lambda_j}\ln\gamma_j \tag{31}$$

where λ_j represents the state transition rate of component j. If component j is in the work state, λ_j is the failure rate of component j, whereas if component j is in the outage state, λ_j is the repair rate of component j.

The state sequence of each component can be obtained by repeating (31).

The wind power output sequence generated as described in section IV.A should be updated based on the simulated state sequence of the wind power unit. If the wind power unit is in the outage state at time t, then its wind power output at time t is zero. If the wind power unit is in the work state at time t, then its wind power output at time t remains unchanged. Furthermore, the reliability model of wind farms can also be simplified as a two-state model.

C. Calculation of the Unreliability Tracing Index

1) Calculation of Risk Factors

The method for generating the wind power output is described in section IV.A, the aleatory and epistemic uncertainties of the wind power output are characterized by two independent random variables u_1^w and u_2^w, respectively, which are uniformly distributed in [0, 1]. u_1^w and u_2^w have the same dimensions as the unreliability index function $g(\boldsymbol{x})$ and each corresponds to a certain value at each sample time t, thus generating the wind power output sequence of the sample period T.

Although the component state sequence generated by the sequential MCS method in section IV.B can characterize the uncertainty of component outages, the state duration does not correspond to the sample period T. To homogenize and integrate the uncertainty of component outages into the unified tracing unreliability procedure, the model in section IV.B needs to be multistated.

Suppose that a sufficiently long component state sequence with the length of T_{com} is simulated as described in section IV.B. Then, the component state sequence is truncated to the length of each sample period T. In this way, a total of N_{com} sequential state segments can be obtained, and N_{com} can be calculated as follows:

$$N_{\text{com}} = \frac{T_{\text{com}}}{T} \tag{32}$$

$\partial_{j,k_{\text{com}}}$ and s_j represent the state segment k_{com} and the state of component j, respectively, in a certain sample period. A random number u_3^j uniformly distributed in [0, 1] is generated for component j; thus, s_j can be calculated as follows:

$$s_j = \begin{cases} \partial_{j,1}, 0 \leqslant u_3^j \leqslant \dfrac{1}{N_{\text{com}}} \\ \vdots \\ \partial_{j,k_{\text{com}}}, \dfrac{k_{\text{com}}-1}{N_{\text{com}}} \leqslant u_3^j \leqslant \dfrac{k_{\text{com}}}{N_{\text{com}}} \\ \vdots \\ \partial_{j,N_{\text{com}}}, \dfrac{N_{\text{com}}-1}{N_{\text{com}}} \leqslant u_3^j \leqslant 1 \end{cases} \tag{33}$$

Therefore, $\boldsymbol{u}_1$ (the set of u_1^w representing aleatory uncertainty of wind power output), $\boldsymbol{u}_2$ (the set of u_2^w representing epistemic uncertainty of wind power output), and $\boldsymbol{u}_3$ (the set of u_3^j representing the uncertainty of component outages) during the sample period T, corresponding to the three kinds of risk factors, together constitute the risk factor set $\boldsymbol{x}$:

$$\boldsymbol{x} = \{\boldsymbol{u}_1, \boldsymbol{u}_2, \boldsymbol{u}_3\} \tag{34}$$

2) Calculation of the Unreliability Index Function

The unreliability index function $g(\boldsymbol{x})$ should be calculated for each risk factor sample using the optimal power flow (OPF)-based model [40]:

$$g(\boldsymbol{x}) = \min \sum_{i=1}^{N_{\text{bus}}} \sum_{t=1}^{T} P_{i,t}^{\text{cur}} \tag{35}$$

s.t.

$$\boldsymbol{h}_{\text{ieq}}(\boldsymbol{\theta}, \boldsymbol{P}^{\text{tu}}, \boldsymbol{P}^{\text{wind}}, \boldsymbol{P}^{\text{cur}}) \leqslant 0 \tag{36}$$

$$\boldsymbol{h}_{\text{ieq}}(\boldsymbol{\theta}, \boldsymbol{P}^{\text{tu}}, \boldsymbol{P}^{\text{wind}}, \boldsymbol{P}^{\text{cur}}) = 0 \tag{37}$$

where $P_{i,t}^{\text{cur}}$ denotes the load shedding of bus i at time t. The number of buses is N_{bus} and the sample period T is 24 h. The decision variables include the sets of bus phase angles $\boldsymbol{\theta}$, the thermal unit outputs $\boldsymbol{P}^{\text{tu}}$, the wind power outputs $\boldsymbol{P}^{\text{wind}}$, and the electric load shedding $\boldsymbol{P}^{\text{cur}}$.

The objective function in (35) is designed to minimize the load shedding of the power system.

Equation (36) denotes the inequality constraints of the OPF-based model, including the limits of transmission line capacity, generation and ramping capacity of thermal units, wind power unit capacity, load shedding, and phase angles, which are shown as follows:

$$\left|(\theta_{i,t} - \theta_{i',t}) / X_{i,i'}\right| \leqslant F_{i,i'}^{\max} s_{ii',t}, \forall i, i' \in \boldsymbol{B}, \forall t \in \boldsymbol{T} \tag{38}$$

$$P_g^{\text{tu,min}} s_{g,t} \leqslant P_{g,t}^{\text{tu}} \leqslant P_g^{\text{tu,max}} s_{g,t}, \forall g \in \boldsymbol{G}, \forall t \in \boldsymbol{T} \tag{39}$$

$$R_g \leqslant P_{g,t}^{\text{tu}} - P_{g,t-\Delta t}^{\text{tu}} = \leqslant U_g, \forall g \in \boldsymbol{G}, \forall t \in \boldsymbol{T} \tag{40}$$

$$P_{w,t}^{\text{wind,min}} s_{w,t} \leqslant P_{w,t}^{\text{wind}} \leqslant P_{w,t}^{\text{wind,max}} s_{w,t}, \forall w \in \boldsymbol{W}, \forall t \in \boldsymbol{T} \tag{41}$$

$$0 \leqslant P_{i,t}^{\text{cur}} \leqslant P_{i,t}^{\text{load}}, \forall i \in \boldsymbol{B}, \forall t \in \boldsymbol{T} \tag{42}$$

$$-\theta_i^{\max} \leqslant \theta_{i,t} \leqslant \theta_i^{\max}, \forall i \in \boldsymbol{B}, \forall t \in \boldsymbol{T} \tag{43}$$

where $\theta_{i,t}$ and $\theta_{i',t}$ denote the phase angles of buses i and i' at time t; $X_{i,i'}$ and $F_{i,i'}^{\max}$ denote the reactance and

maximum capacity of the transmission line connecting buses i and i'; $s_{ii',t}$, $s_{g,t}$, and $s_{w,t}$ denote the binary variables to indicate the states of the transmission line connecting buses i and i', thermal unit g, and wind power unit w, respectively. If the binary variable equals 0, the corresponding component is in the outage state, and the maximum and minimum capacities equal 0; otherwise, the capacities remain unchanged. $P_g^{\text{tu,min}}$ and $P_g^{\text{tu,max}}$, $P_{w,t}^{\text{wind,min}}$ and $P_{w,t}^{\text{wind,max}}$ represent the minimum and maximum outputs of thermal unit g and wind power unit w, respectively; U_g and R_g denote the upwards and downwards ramping capabilities of thermal unit g, respectively; $\theta_i^{\max}$ denotes the maximum phase angle of bus i; $P_{g,t}^{\text{tu}}$, $P_{g,t-\Delta t}^{\text{tu}}$, $P_{w,t}^{\text{wind}}$, and $P_{i,t}^{\text{load}}$ represent the outputs of thermal unit g at time t, $t-\Delta t$, wind power unit w at time t, and the power load of bus i at time t, respectively. $\boldsymbol{B}$, $\boldsymbol{T}$, $\boldsymbol{G}$, and $\boldsymbol{W}$ denote the sets of buses, sample time intervals, thermal units and wind power units, respectively.

Equation (37) denotes the equality constraints of the OPF-based model comprising the DC power flow balance for each bus, which is shown as follows:

$$\sum(\theta_{i,t}-\theta_{i',t})/X_{i,i'}+P_{i,t}^{\text{load}}-P_{i,t}^{\text{cur}}=\sum_{g\in\boldsymbol{G}_i}P_{g,t}^{\text{tu}}+\sum_{w\in\boldsymbol{W}_i}P_{w,t}^{\text{wind}},\forall i,i'\in\boldsymbol{B},\forall t\in\boldsymbol{T} \tag{44}$$

where $\boldsymbol{G}_i$ and $\boldsymbol{W}_i$ denote the sets of thermal units and wind power units connected to bus i, respectively.

Then, with N_{sam} samples, the unreliability index EENS can be expressed as follows:

$$EENS=\frac{365}{N_{\text{sam}}}\sum_{k_{\text{sam}}=1}^{N_{\text{sam}}}g(\boldsymbol{x}_{(k_{\text{sam}})}) \tag{45}$$

3) Calculation of the Unreliability Tracing Index

The MCS process is used to generate two risk factor sample sets $\boldsymbol{\zeta}^1$ and $\boldsymbol{\zeta}^2$, each of which includes N_{sam} samples with N_{obj} risk factors. The dimensions of each sample set are $N_{\text{sam}}\times N_{\text{obj}}$, and $\boldsymbol{\zeta}^3$ is the combined sample set of $\boldsymbol{\zeta}^1$ and $\boldsymbol{\zeta}^2$.

Based on (26) and (27), the average g_0 and variance D of $g(\boldsymbol{x})$ can be calculated as follows:

$$g_0\approx\frac{1}{2N_{\text{sam}}}\sum_{k_{\text{sam}}=1}^{2N_{\text{sam}}}g(\boldsymbol{\zeta}_{k_{\text{sam}}}^3) \tag{46}$$

$$D\approx\frac{1}{2N_{\text{sam}}}\sum_{k_{\text{sam}}=1}^{2N_{\text{sam}}}g^2(\boldsymbol{\zeta}_{k_{\text{sam}}}^3)-g_0^2 \tag{47}$$

where $\boldsymbol{\zeta}_{k_{\text{sam}}}^3$ represents the sample k_{sam} of sample set $\boldsymbol{\zeta}^3$.

Based on sample sets $\boldsymbol{\zeta}^1$ and $\boldsymbol{\zeta}^2$, a new risk factor sample set $\boldsymbol{\eta}^{(v)}$ for each risk factor x_v is defined. The sample set $\boldsymbol{\eta}^{(v)}$ includes N_{sam} samples with N_{obj} risk factors. The value of each sample in the sample set $\boldsymbol{\eta}^{(v)}$ can be obtained as follows:

$$\eta_{k_{\text{sam}},o}^{(v)}=\begin{cases}\boldsymbol{\zeta}_{k_{\text{sam}},o}^1, & o=1,2,\cdots,N_{\text{obj}}\text{ and }o\neq v\\ \boldsymbol{\zeta}_{k_{\text{sam}},o}^2, & o=v\end{cases},\quad \forall k_{\text{sam}}\in\{1,2,\cdots,N_{\text{sam}}\},\forall v\in\{1,2,\cdots,N_{\text{obj}}\} \tag{48}$$

where $\eta_{k_{\text{sam}},o}^{(v)}$, $\boldsymbol{\zeta}_{k_{\text{sam}},o}^1$ and $\boldsymbol{\zeta}_{k_{\text{sam}},o}^2$ represent the sample values in row k_{sam} and column o of sample sets $\boldsymbol{\eta}^{(v)}$, $\boldsymbol{\zeta}^1$ and $\boldsymbol{\zeta}^2$, respectively.

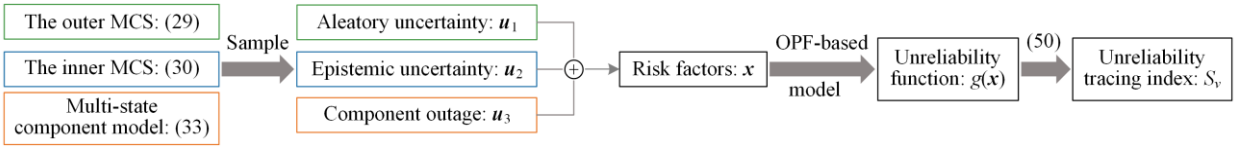

Fig. 5. The calculation procedure of unreliability tracing index.

Based on (28), with sufficient samples, D_v can be approximated as:

$$D_v\approx\frac{1}{N_{\text{sam}}}\sum_{k_{\text{sam}}=1}^{N_{\text{sam}}}g(\boldsymbol{\zeta}_{k_{\text{sam}}}^2)\left[g(\boldsymbol{\eta}_{k_{\text{sam}}}^{(v)})-g(\boldsymbol{\zeta}_{k_{\text{sam}}}^1)\right] \tag{49}$$

where $\boldsymbol{\eta}_{k_{\text{sam}}}^{(v)}$, $\boldsymbol{\zeta}_{k_{\text{sam}}}^1$ and $\boldsymbol{\zeta}_{k_{\text{sam}}}^2$ represent the k_{sam}-row of sample sets $\boldsymbol{\eta}^{(v)}$, $\boldsymbol{\zeta}^1$ and $\boldsymbol{\zeta}^2$, respectively.

In summary, the unreliability tracing index of risk factor x_v can be estimated as follows [39]:

$$S_v\approx\frac{2\sum_{k_{\text{sam}}=1}^{N_{\text{sam}}}g(\boldsymbol{\zeta}_{k_{\text{sam}}}^2)\left[g(\boldsymbol{\eta}_{k_{\text{sam}}}^{(v)})-g(\boldsymbol{\zeta}_{k_{\text{sam}}}^1)\right]}{\sum_{k_{\text{sam}}=1}^{2N_{\text{sam}}}g^2(\boldsymbol{\zeta}_{k_{\text{sam}}}^3)-g_0^2} \tag{50}$$

The unreliability tracing index calculation procedure is shown in Fig. 5. The purpose of the unreliability tracing index is to evaluate the contributions of individual risk factors to the system load-shedding risk.

During the procedure, the number of samples N_{sam} can be increased sequentially until the maximum variability coefficient ε of $S_v\left(S_v\in\left\{S_1,S_2,\ldots,S_{N_{\text{obj}}}\right\}\right)$ satisfies the following convergence requirements:

$$\varepsilon=\max\left(\frac{\sigma(S_v)}{\bar{S}_v}\right)\times100\%\leqslant\varepsilon_{\text{set}} \tag{51}$$

where $\sigma(S_v)$ and $\bar{S}_v$ denote the standard deviation and mean of S_v, respectively; and ε_{set} denotes the convergence value of ε.

4) Unreliability Tracing Flowchart

The algorithm flowchart for unreliability tracing is shown in Fig. 6. The specific steps are as follows:

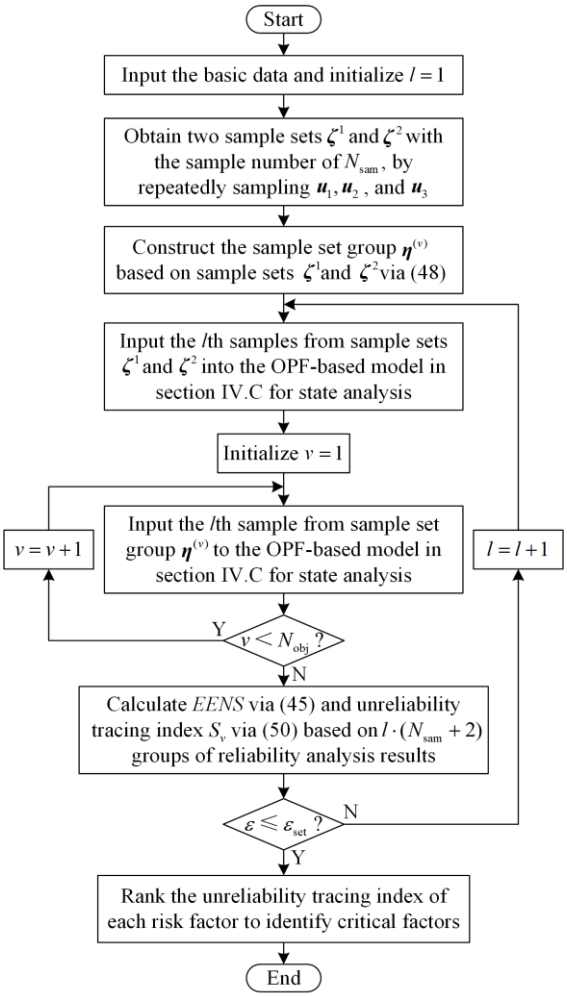

Fig. 6. Flowchart for unreliability tracing for power systems integrated with wind power.

Step 1: Input the basic data of the power system and initialize $l=1$.

Step 2: Obtain two sample sets ζ^1 and ζ^2, each with the sample number of N_{sam}, by sampling u_1, u_2, and u_3 during the sample period T repeatedly.

Step 3: Construct the sample set $\eta^{(v)}$ based on sample sets ζ^1 and ζ^2 via (48).

Step 4: Input sample l from sample sets ζ^1 and ζ^2 into the OPF-based model in section IV.C for system state analysis.

Step 5: Initialize $v=1$.

Step 6: Input sample l from sample set group $\eta^{(v)}$ into the OPF-based model in section IV.C for system state analysis.

Step 7: If $v<N_{sam}$, let $v=v+1$ and go to step 6; otherwise, go to step 8.

Step 8: Calculate the system unreliability index via (45) and the unreliability tracing index S_v via (50) based on the $l\cdot(N_{sam}+2)$ groups of unreliability analysis results.

Step 9: If the maximum variability coefficient ε of S_v satisfies (51), go to step 10; otherwise, let $l=l+1$ and go to step 4.

Step 10: Rank the unreliability tracing index values to identify the most critical risk factors for the power system.

V. Case Study

The proposed unreliability tracing method for power systems integrated with wind power is applied to an improved IEEE-RTS79 system [41]. The specific enhancements to the system are to replace three thermal units at bus 13 and one nuclear unit at bus 21 with four wind farms. The parameters of the wind farms are shown in Table I. The EENS is selected as a representative unreliability index function for analysis.

TABLE I
Parameters of The Wind Farms

Wind farm number	Connected bus	Capacity (MW)	Number of wind power units	MTTF of wind power units (hour)	MTTR of wind power units (hour)
1	13	1.5	130	6041	257
2	13	1.5	130	3000	257
3	13	1.5	260	6041	257
4	21	1.5	520	6041	257

First, to prove the effectiveness of the proposed method, the system unreliability is allocated to conventional units considering component outages and wind farms considering component outages as well as aleatory and epistemic uncertainties of the wind power output. Second, the contributions of the wind farms are further allocated to component outage and wind power output uncertainty, reflecting the contribution of wind power output uncertainty to system unreliability. Finally, the contribution of wind power output uncertainty is allocated to aleatory uncertainty and epistemic uncertainty, and the specific contribution of epistemic uncertainty to system unreliability is analysed.

A. Unreliability Tracing Results for Conventional Components and Wind Farms

1) Unreliability Tracing Results of the Proportional Allocation Method and the Proposed Method

Table II and Table III present the unreliability tracing results of the proportional allocation method and the proposed method based on EENS analysis, respectively. The results are expressed in terms of the rank of the unreliability tracing indices. For ease of analysis and illustration, only the top 10 most critical components are given. In addition, Fig. 7 compares the EENS-based unreliability tracing indices of the six components that

rank in the top 10 based on both unreliability tracing methods.

As shown in Table II, the unreliability tracing indices of components obtained via the proportional allocation method tend to decrease with decreasing forced outage rates (FORs). This is due to one of the two basic principles of the proportional allocation method [13]: the load-shedding risk is allocated proportionally to each relevant component in accordance with their reliability parameters.

TABLE II
UNRELIABILITY TRACING RESULTS BASED ON THE PROPORTIONAL ALLOCATION METHOD

Rank	Component	Connected bus	Capacity (MW)	FOR	Unreliability tracing index (%)
1	Unit 31	18	400	0.12	21.44
2	Unit 30	23	350	0.08	9.78
3	Unit 6	1	20	0.10	3.12
4	Unit 7	1	20	0.10	3.12
5	Unit 8	2	20	0.10	3.12
6	Unit 9	2	20	0.10	3.12
7	Wind farm 2	13	195	0.08	3.03
8	Wind farm 4	21	800	0.04	2.95
9	Unit 23	15	155	0.04	2.37
10	Unit 24	16	155	0.04	2.37

TABLE III
UNRELIABILITY TRACING RESULTS BASED ON THE PROPOSED METHOD

Rank	Component	Connected bus	Capacity (MW)	FOR	Unreliability tracing index (%)
1	Unit 31	18	400	0.12	20.84
2	Wind farm 4	21	800	0.04	11.13
3	Unit 30	23	350	0.08	9.31
4	Wind farm 3	13	390	0.04	3.65
5	Unit 23	15	155	0.04	2.09
6	Unit 24	16	155	0.04	1.97
7	Unit 25	23	155	0.04	1.66
8	Unit 26	23	155	0.04	1.66
9	Wind farm 2	13	195	0.08	1.65
10	Wind farm 1	13	195	0.04	1.35

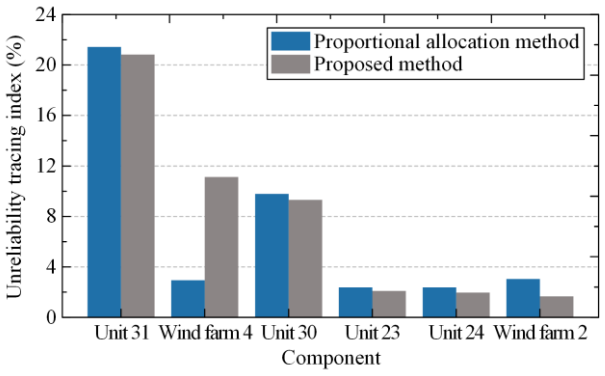

Fig. 7. Unreliability tracing results based on the proportional allocation method and the proposed method.

However, unreliability tracing based solely on component reliability parameters lacks impartiality. For example, the FOR of unit 23 is lower than that of unit 6, but the capacity of unit 23 is greater. If unit 23 and unit 6 are in the outage state at the same time, unit 23 should make a greater contribution to the load-shedding event. However, unit 23 ranks lower than unit 6 in Table II, indicating that unreliability tracing based only on the components' reliability parameters will lead to unreasonable results. Specifically, in Table II, units 6–9 with low capacities and high FORs, are unreasonable for ranking higher in the unreliability tracing index than other units with significantly larger capacities.

In addition, in some load-shedding events, the outage of some components may not contribute to load shedding. For example, there are two transmission lines, 36 and 37, connecting buses 23 and 20. Suppose that in a load-shedding event, unit 25 and unit 26 at bus 23 and transmission line 36 are in the outage state simultaneously, while transmission line 37 works normally. Unless the power flow is off-limit, the outage of transmission line 36 will not contribute to the load-shedding event. Thus, it is unreasonable to allocate the load-shedding risk to these three outage components in accordance with the reliability parameters of the components, as in the proportional allocation method.

Moreover, the sum of the unreliability tracing indices obtained under the proportional allocation method is only approximately 80%. This is due to the second basic principle of the proportional allocation method [13]: only components in the outage state contribute to load-shedding events.

However, in some load-shedding events in power systems integrated with wind power, there is no component in the outage state; thus, the system load shedding is caused solely by the wind power output uncertainty. Specifically, due to a lack of ramping ability, the system may be unable to compensate for the wind power output uncertainty, thus leading to load shedding. This kind of load-shedding risk cannot be allocated via the proportional allocation method. Thus, the effectiveness of the unreliability tracing results and any reliability enhancement strategy based on them will be suspected.

In contrast to the results of the proportional allocation method, the sum of the unreliability tracing indices obtained under the proposed method is close to 100%, indicating the feasibility and validity of the proposed method.

2) Reliability Enhancement Strategies Based on the Unreliability Tracing Results

To validate the effectiveness of the proposed method, reliability enhancement strategies are proposed based on the unreliability tracing results of both the proportional allocation method and the proposed method. The specific strategy is to reduce the failure rate by 20% and improve the repair rate by 20% for components ranked

1–4, and to reduce the failure rate by 5% and improve the repair rate by 5% for components ranked 5–10.

The system unreliability indices after the reliability enhancement strategies are shown in Table IV.

TABLE IV
RELIABILITY ENHANCEMENT PERFORMANCE

Method	EENS (MW/year)	EENS reduction (%)
Original system	6.73×10^5	
Proportional allocation method	5.91×10^5	12.18
Proposed method	5.54×10^5	17.68

Table IV shows that the unreliability index after the reliability enhancement strategy based on the proposed method is smaller than that after the strategy based on the proportional allocation method. Specifically, the system EENS is significantly reduced by 17.68% after the strategy based on the proposed method.

Thus, it is proven that the reliability enhancement strategy based on the unreliability tracing results of the proposed method has obvious advantages, indicating that the proposed method is more effective and reasonable.

B. Unreliability Tracing Results for Component Outage and Wind Power Output Uncertainty

To measure the influence of the wind power output on the adequacy of the power system capacity, the concept of the wind power capacity credit is proposed.

The wind power capacity credit refers to the proportion of conventional unit capacity that can be replaced by wind power units while keeping the system reliability unchanged.

It is generally believed that the wind power capacity credit is between 20% and 30%. In the case study, the wind power capacity credit is assumed to be 25%.

Based on the wind power capacity credit, wind farm 3 can be considered approximately equivalent to a conventional unit with a capacity of 97.5 MW. However, as shown in Table III, its unreliability tracing index is greater than those of units 23–26 with the same FOR, each of which has a capacity of 155 MW.

Therefore, the unreliability tracing index of a wind farm is much greater than that of a conventional unit with similar capacity after wind power capacity credit conversion. This is because, after the large-scale integration of wind power, system load shedding is caused not only by inadequacy but also by variability, mainly resulting from the uncertainty of wind power output. The unreliability tracing indices of the four wind farms can be further subdivided as shown in Fig. 8.

It can be seen in Fig. 8 that, the unreliability tracing index of wind power output uncertainty is 2–3 times that of component outages, indicating that wind power output uncertainty is more noteworthy for power systems integrated with wind power.

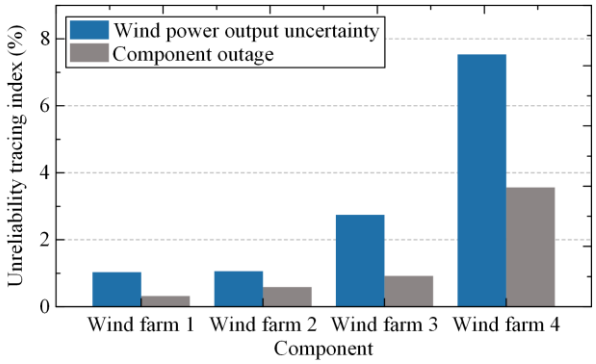

Fig. 8. Unreliability tracing results for risk factors related to wind power.

C. Unreliability Tracing Results for the Aleatory Uncertainty and Epistemic Uncertainty of Wind Power Output

As seen from section V.B, the wind power output uncertainty contributes greatly to the system load-shedding risk. In addition, wind power output uncertainty can be further divided into aleatory uncertainty and epistemic uncertainty. Aleatory uncertainty is determined by the inherent fluctuations of wind, which cannot be artificially adjusted. However, epistemic uncertainty is caused by incomplete knowledge, which can be reduced by artificial means.

Therefore, the unreliability tracing index corresponding to the wind power output uncertainty is further subdivided into indices corresponding to aleatory and epistemic uncertainties, as shown in Fig. 9.

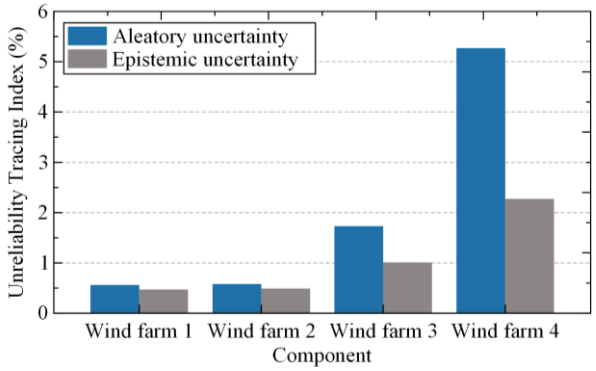

Fig. 9. Unreliability tracing results for the aleatory and epistemic uncertainties of the wind power output.

As shown in Fig. 9, the unreliability tracing indices corresponding to the aleatory uncertainty and epistemic uncertainty of wind farms 1 and 2 are identical. This is because they are connected to the same bus and have the same capacity; thus, the distributions of the associated uncertainties are identical. However, as shown in Fig. 8, the unreliability tracing index of component outage for wind farm 2 is greater than that for wind farm 1. This is due to the greater FOR of wind farm 2 than that of wind farm 1.

The unreliability tracing indices of component outage, aleatory uncertainty, and epistemic uncertainty for wind farms 1, 3, and 4 increase successively. This is because their capacities increase successively with the same FOR. Moreover, the unreliability tracing index corresponding to aleatory uncertainty increases the fastest, indicating that the share of unreliability contributed by wind fluctuations increases with increasing wind farm capacity.

D. Influence of Epistemic Uncertainty on System Unreliability

Three different levels of epistemic uncertainty are considered by adjusting the amount of data. The level used in sections V.A–V.C is 50%. A level of 0% represents a precise model with sufficient data, while a level of 100% represents an inaccurate model based on very little data. The system unreliability indices with different levels of epistemic uncertainty are shown in Table V.

TABLE V
RELIABILITY ENHANCEMENT PERFORMANCE

Epistemic uncertainty level (%)	EENS (MW/year)	EENS reduction (%)
100	6.99×10^5	
50	6.73×10^5	3.72
0	6.44×10^5	7.87

As shown in Table V, the EENS decreases as the epistemic uncertainty level decreases, and it is significantly reduced by 7.87% with the elimination of epistemic uncertainty.

These findings prove that the system reliability can be improved by reducing the epistemic uncertainty level. This is due to the wind power output model uncertainty caused by epistemic uncertainty, which the power system lacks the ramping ability to compensate for, thus resulting in system unreliability.

Taking wind farm 4 as an example, the influence of epistemic uncertainty on unreliability tracing is further analysed in Fig. 10, where the size of the pie chart represents the magnitude of the unreliability tracing index of wind farm 4.

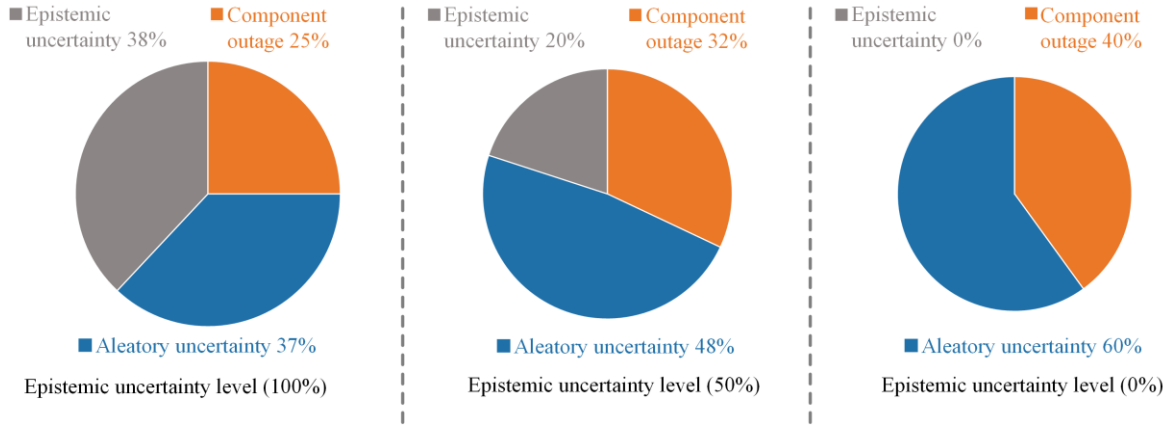

Fig. 10. Unreliability tracing results with different levels of epistemic uncertainty.

As shown in Fig. 10, the unreliability tracing index associated with epistemic uncertainty decreases with decreasing epistemic uncertainty. However, the ratio between the indices associated with aleatory uncertainty and component outage remains at 3:2, indicating that the change in the epistemic uncertainty level does not influence the unreliability contribution of aleatory uncertainty and component outage for the same wind farm.

VI. CONCLUSIONS

In this paper, a novel unreliability tracing model is developed for identifying the most critical risk factors in power systems integrated with wind power. First, models of multisource heterogeneous factors are established through a full analysis of different characteristics of the risk factors for power systems integrated with wind power. Then, based on ANOVA theory, an unreliability tracing index is established to measure the contributions of individual risk factors to the system load-shedding risk. Finally, a novel unreliability tracing method for power systems integrated with wind power is proposed.

The simulation results verify that the proposed method can effectively identify the critical risk factors associated with power system load shedding and thereby guide the development of targeted reliability enhancement strategies.

Guided by the proposed unreliability tracing method, the corresponding enhancement strategy reduces the EENS by 17.68%, which is 1.5 times the reduction achieved based on the traditional proportional allocation method. This demonstrates that the proposed method provides more accurate results than the traditional method. Moreover, wind power output uncertainty has a significant detrimental impact on power system reliability, which is even greater than that of component outages. Specifically, the unreliability tracing index associated with wind power output uncertainty is 2–3

times that associated with component outages. In addition, the EENS significantly decreases by 7.87% when wind power epistemic uncertainty is eliminated, indicating the effectiveness of enhancing system reliability by eliminating epistemic uncertainty.

ACKNOWLEDGMENT

Not applicable.

AUTHORS' CONTRIBUTIONS

Siyang Zhao: writing-original draft, conceptualization, methodology, validation, and formal analysis. Changzheng Shao: writing-review and editing and formal analysis. Jinfeng Ding: conceptualization, methodology, and validation. Bo Hu and Kaigui Xie: supervision. Xueying Yu and Zihan Zhu: writing-review and editing. All authors read and approved the final manuscript.

FUNDING

This work is supported by the National Natural Science Foundation of China (No. 52107072) and the Natural Science Foundation of Chongqing (No. CSTB2022NSCQ-MSX0811).

AVAILABILITY OF DATA AND MATERIALS

Not applicable.

DECLARATIONS

Competing interests: The authors declare that they have no known competing financial interests or personal relationships that could have appeared to influence the work reported in this article.

AUTHORS' INFORMATION

Siying Zhao received the M.S. degree in electrical engineering from Chongqing University, Chongqing, China, in 2024. She is currently an assistant designer with the Hubei Electric Power Planning, Design and Research Institute Co., Ltd., Wuhan, China. Her current research interests include the reliability of power systems and integrated energy systems.

Changzheng Shao received the Ph.D. degree in electrical engineering from Zhejiang University, Zhejiang, China, in 2020. He is currently an associate professor with Chongqing University, Chongqing, China. His research interests include the operation optimization and reliability evaluation of integrated energy system.

Jinfeng Ding received the B.S. and M.S. degrees in electrical engineering from Chongqing University, Chongqing, China, in 2019 and 2022, respectively. He is currently an engineer at State Grid Chengdu Electric Power Supply Company, Sichuan, China. His research interests include power system reliability evaluation, renewable energy, and power system optimization.

Bo Hu received the Ph.D. degree in electrical engineering from Chongqing University, Chongqing, China, in 2010. He is currently a professor with the School of Electrical Engineering, Chongqing University. His research interests include power system reliability and parallel computing techniques in power systems.

Kaigui Xie received the Ph.D. degree in power system and its automation from Chongqing University, Chongqing, China, in 2001. He is currently a full professor with the School of Electrical Engineering, Chongqing University. His main research interests include power system reliability, planning, and analysis. He is the editor of the IEEE Transactions on Power Systems.

Xueying Yu received the Ph.D. degree in electrical engineering from Chongqing University, Chongqing, China, in 2023. She is currently a postdoctor in electrical engineering from Sichuan University, Sichuan, China. Her research interests encompass the reliability evaluation of generation systems integrated with renewable energy.

Zihan Zhu received the B.S. degree in electrical engineering from Guizhou University, Guizhou, China, in 2022. He is working toward the M.S. degree with the School of Electrical Engineering, Chongqing University, Chongqing, China. His current research interests include day-ahead scenario generation of distribution networks with distributed generation.

REFERENCES

[1] R. G. Smead, "Ercot-the eyes of Texas (and the world) are upon you: What can be done to avoid a February 2021 repeat," *Climate and Energy*, vol. 37, no. 10, pp. 14-18, Oct. 2021.

[2] Z. Wang, T. Hong, and H. Li, "Informing the planning of rotating power outages in heat waves through data analytics of connected smart thermostats for residential buildings," *Environmental Research Letters*, vol. 16, no. 7, Jul. 2021.

[3] O. A. Ansari, C. Y. Chung, and E. Zio, "A novel framework for the operational reliability evaluation of integrated electric power-gas networks," *IEEE Transactions on Smart Grid*, vol. 12, no. 5, pp. 3901-3913, Sep. 2021.

[4] M. Cao, C. Shao, and B. Hu *et al.*, "Reliability assessment of integrated energy systems considering emergency dispatch based on dynamic optimal energy flow," *IEEE Transactions on Sustainable Energy*, vol. 13, no. 1, pp. 290-301, Jan. 2021.

[5] Y. Zhou, X. Li, and H. Han *et al*., "Resilience-oriented planning of integrated electricity and heat systems: a stochastic distributionally robust optimization approach," *Applied Energy*, vol. 353, 2024.
[6] G. Li, G. Huang, and Z. Bie *et al*., "Component importance assessment of power systems for improving resilience under wind storms," *Journal of Modern Power Systems and Clean Energy*, vol. 7, no. 4, pp. 676-687, Jul. 2019.
[7] H. WANG, J. GAO, and J. HUANG *et al*.,"Power system operational reliability evaluation method considering data center load flexibility," *Power System Protection and Control*, vol. 51, no. 21, pp. 96-105, Nov. 2023. (in Chinese)
[8] S. Ouyang, Y. Huang, and M. Yang, "Reliability modeling of multi-terminal DC circuit breaker and its impact on multi-terminal DC distribution network," *International Journal of Electrical Power & Energy Systems*, vol. 147, 2023.
[9] V. C. Mathebula and A. K. Saha, "Reliability of IEC 61850 based substation communication network architecture considering quality of repairs and common cause failures," *Protection and Control of Modern Power Systems*, vol. 7, no. 1, pp. 174-188, Jan. 2022.
[10] H. Bai and S. Miao, "Hybrid flow betweenness approach for identification of vulnerable line in power system," *IET Generation, Transmission & Distribution*, vol. 9, no. 12, pp. 1324-1331, Dec. 2015.
[11] C. Chen, Y. Zhou, and Y. Wang *et al*., "Vulnerable line identification of cascading failure in power grid based on new electrical betweenness," *IEEE Transactions on Circuits and Systems II: Express Briefs*, vol. 70, no. 2, pp. 665-669, Feb. 2022.
[12] D. Deka, S. Vishwanath, and R. Baldick, "Analytical models for power networks: the case of the western US and ERCOT grids," *IEEE Transactions on Smart Grid*, vol. 8, no. 6, pp. 2794-2802, Jun. 2016.
[13] K. Xie and R. Billinton, "Tracing the unreliability and recognizing the major unreliability contribution of network components," *Reliability Engineering & System Safety*, vol. 94, no. 5, pp. 927-931, May 2009.
[14] M. Cao, C. Shao, and B. Hu *et al*., "Reliability tracing of the integrated energy system using the improved Shapley value," *Energy*, vol. 260, 2022.
[15] J. Yang, T. Yang, and L. Luo *et al*., "Tracking-dispatch of a combined wind-storage system based on model predictive control and two-layer fuzzy control strategy," *Protection and Control of Modern Power Systems*, vol. 8, no. 4, pp. 974-989, Oct. 2023.
[16] D. Xiao, H. Chen, and W. Cai *et al*., "Integrated risk measurement and control for stochastic energy trading of a wind storage system in electricity markets," *Protection and Control of Modern Power Systems*, vol. 8, no. 4, pp. 1002-1012, Oct. 2023.
[17] M. Bao, H. Hui, and Y. Ding *et al*., "An efficient framework for exploiting operational flexibility of load energy hubs in risk management of integrated electricity-gas systems," *Applied Energy*, vol. 338, 2023.
[18] H. Hui, M. Bao, and Y. Ding *et al*., "Exploring the integrated flexible region of distributed multi-energy systems with process industry," *Applied Energy*, vol. 311, 2022.
[19] Z. Ma, H. Chen, and Y. Chai, "Analysis of voltage stability uncertainty using stochastic response surface method related to wind farm correlation," *Protection and Control of Modern Power Systems*, vol. 2, no. 3, pp. 211-219, Jul. 2017.
[20] D. Zheng, A. T. Eseye, and J. Zhang *et al*., "Short-term wind power forecasting using a double-stage hierarchical ANFIS approach for energy management in microgrids," *Protection and Control of Modern Power Systems*, vol. 2, no. 2, pp. 136-145, Apr. 2017.
[21] L. Chen, C. Li, and Z. Xin *et al*., "Simulation and risk assessment of power system with cascading faults caused by strong wind weather," *International Journal of Electrical Power & Energy Systems*, vol. 143, 2022.
[22] R. He, X. Li, and G. Chen *et al*., "A quantitative risk analysis model considering uncertain information," *Process Safety and Environmental Protection*, vol. 118, pp. 361-370, 2018.
[23] J. Mi, Y. F. Li, and Y. J. Yang *et al*., "Reliability assessment of complex electromechanical systems under epistemic uncertainty," *Reliability Engineering & System Safety*, vol. 152, pp. 1-15, 2016.
[24] W. Yang, M. Cao, and P. Ge *et al*., "Risk-oriented renewable energy scenario clustering for power system reliability assessment and tracing," *IEEE Access*, vol. 8, pp. 183995-184003, 2020.
[25] X. Yang, Y. Yang, and Y. Liu *et al*., "A reliability assessment approach for electric power systems considering wind power uncertainty," *IEEE Access*, vol. 8, pp. 12467-12478, 2020.
[26] A. Ahmadpour and S. G. Farkoush, "Gaussian models for probabilistic and deterministic wind power prediction: wind farm and regional," *International Journal of Hydrogen Energy*, vol. 45, no. 51, pp. 27779-27791, 2020.
[27] W. H. Lio, A. Li, and F. Meng, "Real-time rotor effective wind speed estimation using Gaussian process regression and Kalman filtering," *Renewable Energy*, vol. 169, pp. 670-686, 2021.
[28] Z. Li, L. Ye, and Y. Zhao *et al*., "Short-term wind power prediction based on extreme learning machine with error correction," *Protection and Control of Modern Power Systems*, vol. 1, no. 1, pp. 9-16, Jan. 2016.
[29] C. Yan, Y. Tang, and J. Dai *et al*., "Uncertainty modeling of wind power frequency regulation potential considering distributed characteristics of forecast errors," *Protection and Control of Modern Power Systems*, vol. 6, no. 3, pp. 276-288, Jul. 2021.
[30] J. Ding, K. Xie, and B. Hu *et al*., "Mixed aleatory-epistemic uncertainty modeling of wind power forecast errors in operation reliability evaluation of power systems," *Journal of Modern Power Systems and Clean Energy*, vol. 10, no. 5, pp. 1174-1183, Sep. 2022.
[31] J. G. McLeish, "Enhancing MIL-HDBK-217 reliability predictions with physics of failure methods," in *Proceedings of Annual Reliability and Maintainability Symposium (RAMS)*, California, USA, Jan. 2010, pp. 1-6.
[32] FIDES Group. "Reliability methodology for electronic systems-FIDES guide," 2009.
[33] D. Zhou, Z. Wang, and P. Jarman *et al*., "Data requisites for transformer statistical lifetime modelling-part II:

Combination of random and aging-related failures," *IEEE Transactions on Power Delivery*, vol. 29, no. 1, pp. 154-160, Jan. 2013.

[34] C. Melchor-Hernández, F. Rivas-Dávalos, and S. Maximov *et al*., "An analytical method to estimate the Weibull parameters for assessing the mean life of power equipment," *International Journal of Electrical Power & Energy Systems*, vol. 64, pp. 1081-1087, 2015.

[35] J. Teh, "Uncertainty analysis of transmission line end-of-life failure model for bulk electric system reliability studies," *IEEE Transactions on Reliability*, vol. 67, no. 3, pp. 1261-1268, Sep. 2018.

[36] S. Lin, X. Sheng, and Y. Xie *et al*., "An uncertain optimal energy flow model for CCHP campus microgrid using parameterized probability boxes," *Journal of Modern Power Systems and Clean Energy*, vol. 11, no. 5, pp. 1618-1633, Sep. 2023.

[37] I. M. Sobol, "Global sensitivity indices for nonlinear mathematical models and their Monte Carlo estimates," *Mathematics and Computers in Simulation*, vol. 55, no. 1-3, pp. 271-280, 2001.

[38] G. Archer, A. Saltelli, and I. M. Sobol, "Sensitivity measures, ANOVA-like techniques and the use of bootstrap," *Journal of Statistical Computation and Simulation*, vol. 58, no. 2, pp. 99-120, Feb. 1997.

[39] S. Tarantola, D. Gatelli, and S. Kucherenko *et al*., "Estimating the approximation error when fixing unessential factors in global sensitivity analysis," *Reliability Engineering & System Safety*, vol. 92, no. 7, pp. 957-960, 2007.

[40] F. Qi, M. Shahidehpour, and F. Wen *et al*., "Decentralized privacy-preserving operation of multi-area integrated electricity and natural gas systems with renewable energy resources," *IEEE Transactions on Sustainable Energy*, vol. 11, no. 3, pp. 1785-1796, Jul. 2020.

[41] Probability Methods Subcommittee, "IEEE reliability test system," *IEEE Transactions on Power Apparatus and Systems*, vol. PAS-98, no. 6, pp. 2047-2054, Nov. 1979.